## A Scheme to Implement a Universal Two-Qubit Quantum Circuit using Cross-Resonance Hamiltonian

M. Karthick Selvan\* and S. Balakrishnan<sup>†</sup>
Department of Physics, School of Advanced Sciences,
Vellore Institute of Technology, Vellore - 632014, Tamilnadu, India.

In this brief report, we propose a circuit which is locally equivalent to a recently proposed universal two-qubit quantum circuit involving two applications of special perfect entanglers (SPEs) and local y-rotations. Further, we discuss a scheme to implement the equivalent circuit using cross-resonance Hamiltonian. We implement the B-gate circuit using a CNOT gate and a  $\sqrt{\text{CNOT}}$  gate. This requires the implementation time which is approximately 64.84% of the time required to implement the same gate using two CNOT gates. We also show that (n-1) applications of B-gate can generate both the n-qubit GHZ state and n-qubit perfect W state.

Universality is an important aspect of entangling two-qubit gates in the circuit model of quantum computation. It implies the ability of an entangling two-qubit gate to simulate an arbitrary n-qubit unitary operation by multiple applications of the entangling two-qubit gate along with suitable single-qubit gates. Universality can be attributed to the nonlocal characteristics of two-qubit gates such as their ability to create entanglement [1].

Usage of an entangling two-qubit gate as universal two-qubit gate relies on the maximum number of its applications required to generate all other two-qubit gates. Three applications of special perfect entanglers (SPEs) are required to generate all two-qubit gates [2]. However, the B-gate is an exemption as it can generate all two-qubit gates in two applications [3]. Universal two-qubit quantum circuits consisting of parameterized two-qubit gates from a family of gates can also be used to generate all two-qubit gates [4]. Recently the circuit equivalence,

$$\hat{\mathbf{U}}_{d}(c_{1}, c_{2}, c_{3}) \sim \hat{\mathbf{U}}_{d}\left(\frac{\pi}{2}, \frac{c_{2}}{2}, 0\right) [\hat{\mathbf{R}}_{y}(c_{1}) \otimes \hat{\mathbf{R}}_{y}(-c_{3})]$$

$$\hat{\mathbf{U}}_{d}\left(\frac{\pi}{2}, \frac{c_{2}}{2}, 0\right)$$
(1)

with  $\hat{R}_y(c_j) = \exp\left(\frac{ic_j\hat{\sigma}_y}{2}\right)$ , where j = 1, 3, was established and the circuit shown in FIG. 1 was proposed as universal two-qubit quantum circuit by the authors [5].

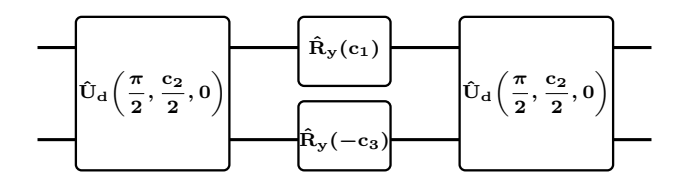


FIG. 1. Universal two-qubit quantum circuit (UTQQC) with two applications of an SPE  $\,$ 

The circuit shown in FIG. 1 involves local y-rotations between two applications of an SPE. All the gates involved in the circuit are single-parameter gates and the gate parameters are the Cartan co-ordinates  $(c_1, c_2, c_3)$ . The Weyl chamber of local equivalence classes of two-qubit gates is shown in FIG. 2.

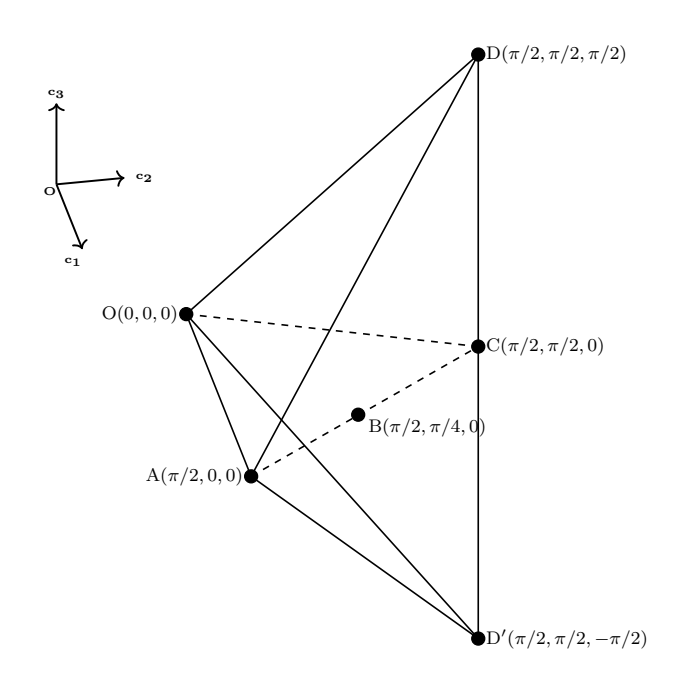


FIG. 2. Weyl chamber: Geometrical representation of local equivalence classes of two-qubit gates.

The Cartan co-ordinates of the local equivalence classes of two-qubit gates represented by the points of Weyl chamber obey the condition:

$$\frac{\pi}{2} \ge c_1 \ge c_2 \ge |c_3| \ge 0.$$

As the parameter of two-qubit gate, the Cartan coordinate  $c_2$ , is changed from 0 to  $\pi/2$ , the circuit employs SPEs represented by the points along the line AB (from CNOT to B-gate local equivalence classes). Without the local operation,  $\hat{R}_v(c_1) \otimes \hat{R}_v(-c_3)$ , as the circuit

 $<sup>^{*}</sup>$  karthick.selvan@yahoo.com

<sup>†</sup> physicsbalki@gmail.com

employs SPEs along the line AB, it generates only the gates represented by the points along the line OA. With local operation,  $\hat{\mathbf{R}}_{\mathbf{y}}(c_1) \otimes \hat{\mathbf{R}}_{\mathbf{y}}(-c_3)$ , between two SPEs, the circuit can generate the gates from all local equivalence classes represented by the points of Weyl chamber by changing the gate parameters.

The allowed values of the parameters of  $R_y$ -gates are decided by the parameter of SPE. For the given SPE corresponding to a specific value of  $c_2$ , the parameters  $c_1$  and  $c_3$  can take values in the closed intervals  $[c_2, \pi/2]$  and  $[-c_2, c_2]$  respectively. Thus for the given SPE with the parameter  $c_2$ , the parameters of the local gates can be changed to generate the gates from local equivalence classes represented by the  $c_2$ -plane of Weyl chamber. But for  $c_2 = 0$  and  $c_2 = \pi/2$ , the local gates of the circuit can only generate the gates represented by the points along the lines OA and DD' respectively. Thus the operation of the circuit can be divided into many  $c_2$  instances. The local equivalence classes of the gates generated by the  $c_2$  instances of UTQQC for eleven equally spaced  $c_2$  values are shown in FIG. 3.

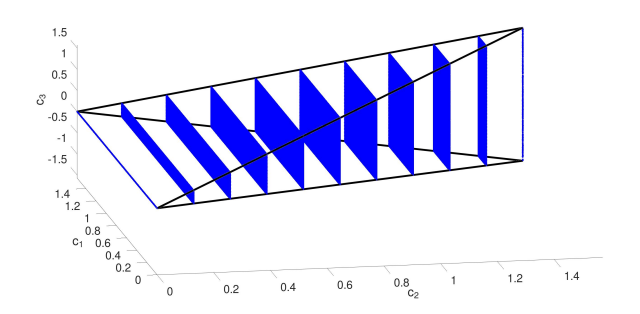


FIG. 3. Regions of Weyl chamber covered by 11 equally spaced  $c_2$  instances of UTQQC. During the  $c_2=0$  and  $c_2=\pi/2$  instances the UTQQC generate gates represented by the edges of the Weyl chamber. The four black lines are the remaining edges of the Weyl chamber.

The implementation of SPEs and hence the UTQQC

(FIG. 1) in ion trap quantum computers was discussed by the authors [5]. Now we propose an equivalent circuit that can be implemented in IBM quantum computers using scaled cross-resonance pulses [7, 8]. In FIG. 4a and 4b, we have shown two circuit equivalences for the SPEs involved in UTQQC. These circuits are the generalization of the B-gate circuit proposed in the Ref. [3].

The single-qubit gate H is the Hadamard gate. The two-qubit gates involved in these circuits are CNOT gate and a gate from  $[\text{CNOT}]^{\alpha}$  family with  $\alpha$  related to the Cartan co-ordinate  $c_2$  as  $\alpha = c_2/\pi$ . When the value of  $c_2$  is changed from 0 to  $\pi/2$ , the value of  $\alpha$  changes from 0 to 0.5.

The circuits on the left hand side (LHS) of FIG. 4a and 4b are not equal to each other but both are locally equivalent to  $\hat{U}(\pi/2, c_2/2, 0)$ . It can be noted that the circuits obtained by swapping the positions of CNOT and [CNOT] $^{c_2/\pi}$  in the circuits on the LHS of FIG. 4 are also locally equivalent to  $\hat{U}(\pi/2, c_2/2, 0)$ . Using these

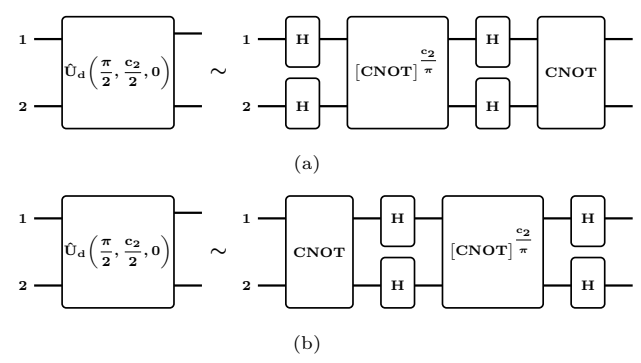


FIG. 4. Circuit equivalences of SPEs

two circuits a UTQQC can be constructed as shown in FIG. 5. In contrary to the UTQQC shown in FIG. 1 the local y-rotations in FIG. 5 are taken as  $\hat{R}_y(c_j) = \exp\left(-\frac{ic_j\hat{\sigma}_y}{2}\right)$ . The universality of the circuit shown in FIG. 5 can be verified by calculating the local invariants of the circuit [6].

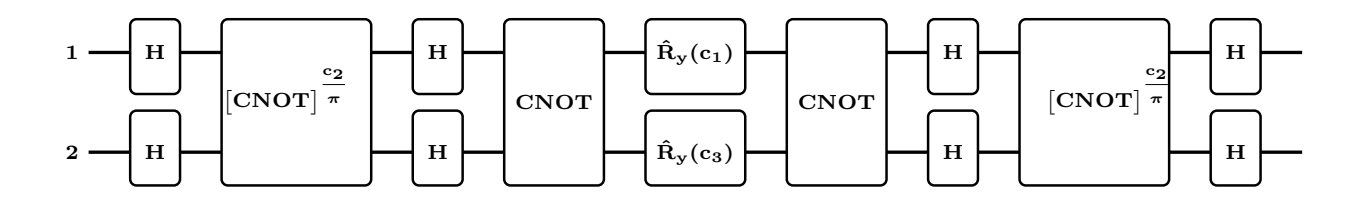


FIG. 5. UTQQC using CNOT gate and gates from [CNOT]<sup> $\alpha$ </sup> family with  $\alpha = c_2/\pi$ .

 $\left[e^{[i\pi(\sigma_z\otimes\sigma_x)/4]}\right]\left[e^{[-i\pi\sigma_z/4]}\otimes e^{[-i\pi\sigma_x/4]}\right]$  where  $\sigma_z$  and  $\sigma_x$  are the Pauli matrices. This product is equal to  $e^{-i\pi/4}[\text{CNOT}]$  with

$$CNOT = \begin{bmatrix} 1 & 0 & 0 & 0 \\ 0 & 1 & 0 & 0 \\ 0 & 0 & 0 & 1 \\ 0 & 0 & 1 & 0 \end{bmatrix}$$
 (2)

The local operator  $\left[e^{[-i\pi\sigma_z/4]}\otimes e^{[-i\pi\sigma_x/4]}\right]$  can be implemented using single-qubit gates. The nonlocal operator  $\left[e^{[i\pi(\sigma_z\otimes\sigma_x)/4]}\right]$  is implemented using the unitary operator

$$U = \exp\left(-itH_{CR}\right)$$

where

$$H_{CR} = \sum_{p=0,x,y,z} \frac{\Omega_{zp}(\sigma_z \otimes \sigma_p)}{2} + \sum_{q=x,y,z} \frac{\Omega_{0q}(\sigma_0 \otimes \sigma_q)}{2}$$
(3)

with  $\sigma_0=I$  is the cross-resonance (CR) Hamiltonian. In addition to  $\sigma_z\otimes\sigma_x$  term, the CR Hamiltonian has six more terms. The unnecessary dominating terms can be eliminated using the techniques discussed in Refs. [9–11] and the operator  $\left[e^{[i\pi(\sigma_z\otimes\sigma_x)/4]}\right]$  can be implemented by choosing  $\frac{\Omega_{zx}t}{2}=-\frac{\pi}{4}$ . The circuit performing the CNOT gate operation between the qubits 0 (control qubit) and 1 (target qubit) of 5-qubit ibmq-quito processor [12] is shown in FIG. 6a.

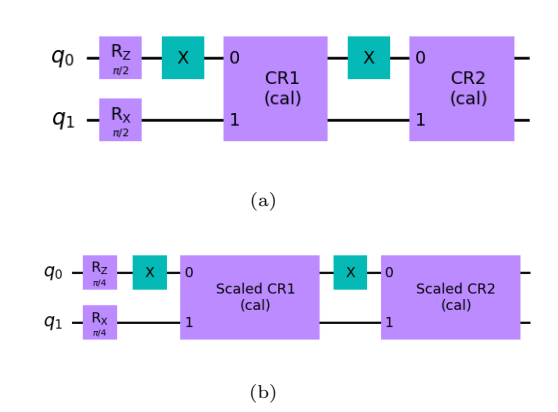
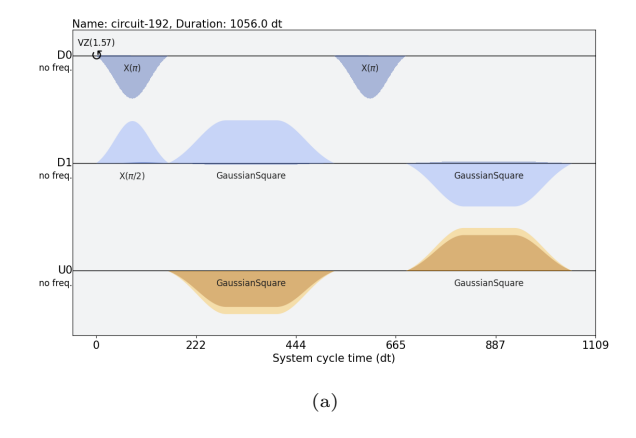


FIG. 6. Circuit performing (a) CNOT operation and (b)  $\sqrt{\text{CNOT}}$  operation.

The local operator  $\left[e^{\left[-i\pi\sigma_{z}/4\right]}\otimes e^{\left[-i\pi\sigma_{x}/4\right]}\right]$  is implemented by applying the single-qubit gates  $R_{z}(\pi/2)$  and  $R_{x}(\pi/2)$  from the circuit library of Qiskit [13] to the qubits 0 and 1 respectively. Two X gates, CR1 and CR2 gates constitute the echoed CR pulse sequence [9–11] corresponding to the CNOT gate. CR1 and CR2 gates contain the compensation pulses on the target qubit in addition to CR pulses. The pulse definitions of CR1 and CR2 gates are defined using Qiskit Pulse and these definitions are assigned to CR1 and CR2 using  $add\_calibration$  method [13]. The pulse sequence corresponding to the CNOT circuit(FIG. 6a) is shown in FIG. 7a.



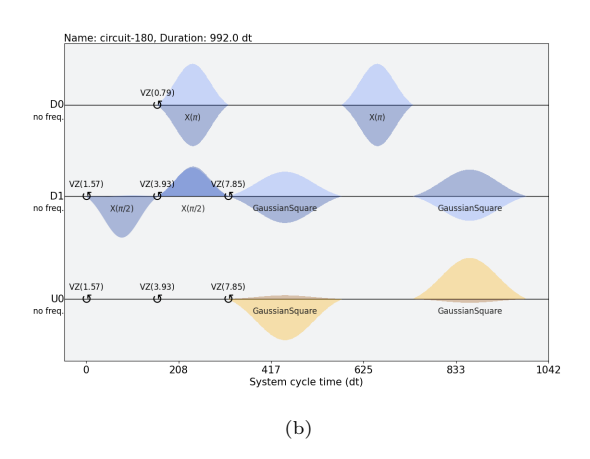


FIG. 7. (a) Pulse sequences of CNOT gate and (b)  $\sqrt{\text{CNOT}}$  gate between the qubits 0 and 1 of 5-qubit ibmq\_quito processor.

Similar to CNOT gate, the gate  $[CNOT]^{c_2/\pi}$  with

 $c_2 \in [0, \pi/2]$  can be implemented as product of unitary

operators  $\left[e^{[ic_2(\sigma_z\otimes\sigma_x)/4]}\right]\left[e^{[-ic_2\sigma_z/4]}\otimes e^{[-ic_2\sigma_x/4]}\right]$  which is equal to the following matrix.

$$e^{-ic_2/4} \begin{bmatrix} 1 & 0 & 0 & 0 \\ 0 & 1 & 0 & 0 \\ 0 & 0 & e^{ic_2/2}\cos(c_2/2) & -ie^{ic_2/2}\sin(c_2/2) \\ 0 & 0 & -ie^{ic_2/2}\sin(c_2/2) & e^{ic_2/2}\cos(c_2/2) \end{bmatrix}$$

The CR pulse used to implement the nonlocal part of CNOT gate has Gaussian square envelope. The nonlocal part  $\left[e^{[ic_2(\sigma_z\otimes\sigma_x)/4]}\right]$  can be implemented by scaling the area of CR pulse as discussed in Ref. [7]. To scale the area of the CR pulse for implementing [CNOT]<sup> $c_2/\pi$ </sup> gate, we consider the following Gaussian square waveform.

$$f(t) = Af'(t)$$

with

$$f'(t) = \begin{cases} \exp\left[-\frac{(t-r)^2}{2\sigma^2}\right], & 0 \le t \le r \end{cases}$$

$$\begin{cases} 1, & r \le t \le r+w \quad (4) \end{cases}$$

$$\left[\exp\left[-\frac{(t-(r+w))^2}{2\sigma^2}\right], & r+w \le t \le d \end{cases}$$

where A is complex amplitude,  $\sigma$  is the standard deviation, w, d and  $r=\frac{d-w}{2}$  are the duration of the embedded square pulse, duration of the entire pulse and risefall duration respectively. The area (S) of the Gaussian square pulse is given by

$$S = |A| \left[ w + \sqrt{2\pi}\sigma \operatorname{erf}\left(\frac{r}{\sqrt{2}\sigma}\right) \right]. \tag{5}$$

To implement  $[CNOT]^{c_2/\pi}$  gate, the area of CR pulse is scaled by following the steps given below.

- The area  $(S_{\text{CNOT}})$  of CR pulse used to implement the CNOT gate is calculated by substituting the pulse parameters in Eq. 5.
- The required area of CR pulse for  $[CNOT]^{c_2/\pi}$  gate is calculated as

$$S_{[\text{CNOT}]^{c_2/\pi}} = \frac{c_2}{\pi} \times S_{\text{CNOT}}.$$
 (6)

Depending on the value of S<sub>[CNOT]<sup>c<sub>2</sub>/π</sup> the pulse parameters w, d and |A| of the CR pulse are modified as discussed in Ref. [7].
</sub>

For qubits 0 and 1 of  $ibmq\_quito$  processor, the value of  $S_{[\text{CNOT}]^{c_2/\pi}}$  with  $c_2=\pi/2$  is found to satisfy the following condition.

$$S_{\sqrt{\text{CNOT}}} < |A_{\text{CNOT}}| \sqrt{2\pi} \sigma \text{erf} \left(\frac{r}{\sqrt{2}\sigma}\right)$$
 (7)

Hence, for the scaled CR pulse, the value of parameter w is taken as zero and consequently the value of d becomes 2r. The amplitude is calculated as

$$|A_{\sqrt{\text{CNOT}}}| = \frac{S_{\sqrt{\text{CNOT}}}}{\sqrt{2\pi}\sigma \text{erf}\left(\frac{r}{\sqrt{2}\sigma}\right)}$$
 (8)

The same procedure is followed for scaling the compensation pulse. The circuit implementing  $\sqrt{\text{CNOT}}$  gate and the corresponding pulse sequence are shown in FIG. 6b and FIG. 7b respectively. The implementation of  $\sqrt{\text{CNOT}}$  gate was reported in Ref. [14].

Using the CNOT and  $\sqrt{\text{CNOT}}$  circuits shown in FIG. 6, the B-gate circuit shown in FIG. 4a (with  $c_2 = \pi/2$ ) can be redrawn as a Qiskit circuit shown in FIG. 8. The corresponding pulse sequence is shown in FIG. 9a. In Qiskit, the same B-gate circuit (FIG. 4a) implements the following unitary matrix.

$$U_B = \frac{1}{2} \begin{bmatrix} 2 & 0 & 0 & 0\\ 0 & 0 & 1 - i & 1 + i\\ 0 & 0 & 1 + i & 1 - i\\ 0 & 2 & 0 & 0 \end{bmatrix}$$
(9)

In Qiskit, this matrix can be directly implemented using 2 CNOT gates and the corresponding pulse sequence is shown in FIG. 9b. It should be mentioned that the implementation time of the circuit shown in FIG. 8 is approximately 64.84% of the implementation time of the unitary matrix  $(U_B)$  using 2 CNOT gates.

The input states  $\{|00\rangle, |01\rangle, |10\rangle, |11\rangle\}$  are transformed by the unitary matrix  $U_B$  as follows.

$$|00\rangle \rightarrow |00\rangle$$

$$|01\rangle \rightarrow |11\rangle$$

$$|10\rangle \rightarrow \frac{e^{-i\pi/4} \left[ |01\rangle + i|10\rangle \right]}{\sqrt{2}}$$

$$|11\rangle \rightarrow \frac{e^{i\pi/4} \left[ |01\rangle - i|10\rangle \right]}{\sqrt{2}}$$
 (10)

We executed the pulse sequence shown in FIG. 9a (corresponding to the B-gate circuit shown in FIG. 8) in  $ibmq\_quito$  processor for all the four input states and measured the output. From the measurement outcomes of 4000 shots, the probability of each outcome is calculated for all four cases and displayed in FIG. 10a. The results almost agree with the transformations shown in Eq. 10. In addition, we executed the pulse sequence shown in FIG. 9b in  $ibmq\_quito$  processor for the input state  $|11\rangle$  and obtained the probabilities for each outcome. In FIG. 10b, we have compared it with the result obtained in the case of pulse sequence shown in FIG. 9a for the same input state. The histogram plot shows that the probabilities are nearly the same in both cases.



FIG. 8. Qiskit implementation of B-gate circuit (FIG. 4a) using CNOT (FIG. 6a) and  $\sqrt{\text{CNOT}}$  (FIG. 6b) gates.

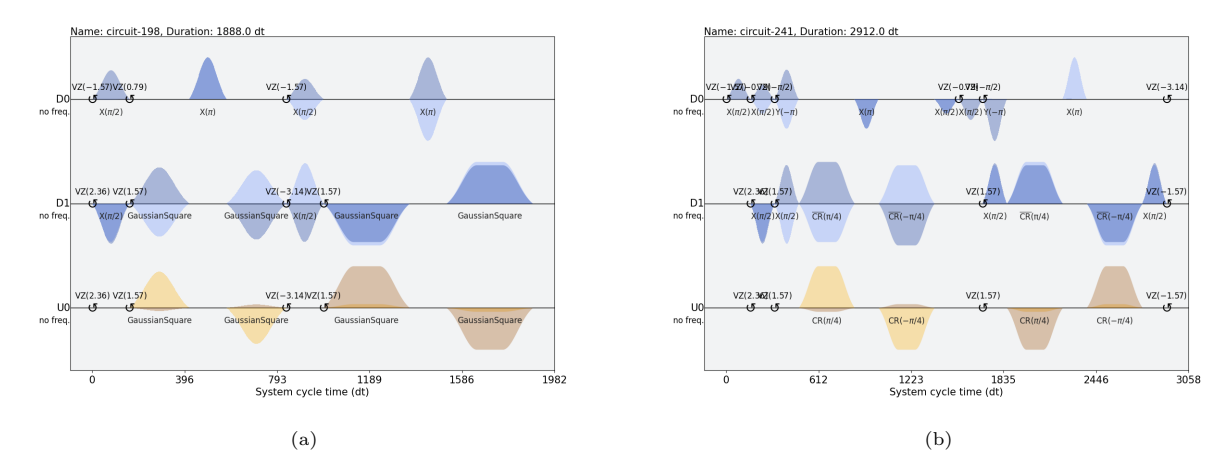


FIG. 9. (a) Pulse sequence of B-gate circuit shown in FIG. 8. (b) Pulse sequence corresponding to the implementation of  $U_B$  (Eq. 9) using 2 CNOT gates.

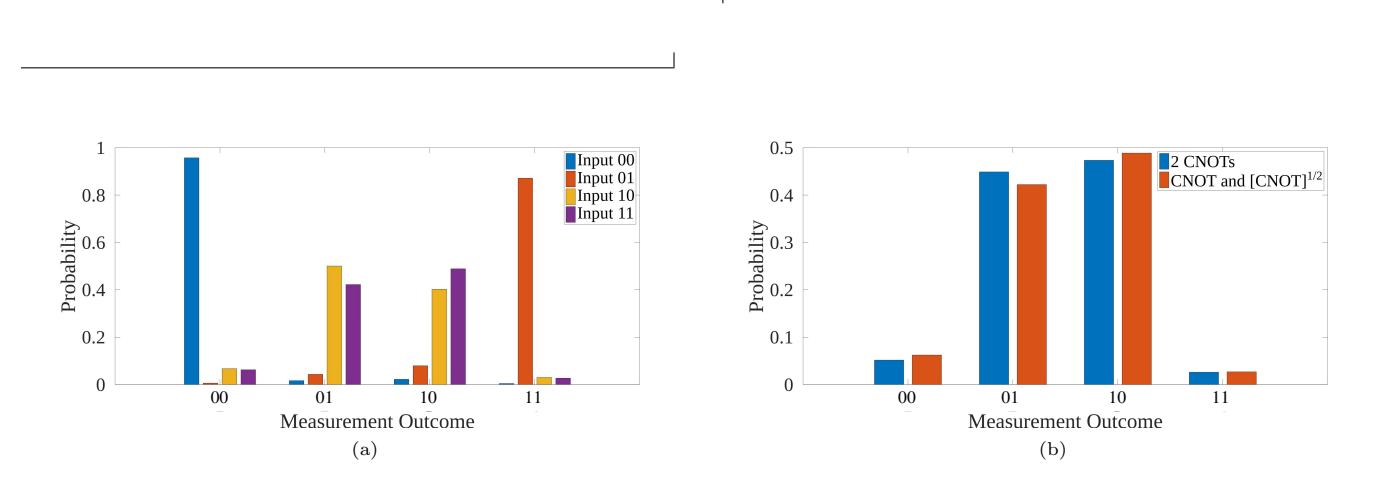


FIG. 10. (a) Probabilities of the measurement outcomes for the pulse sequence shown in FIG. 9a for the input states  $\{|00\rangle, |01\rangle, |10\rangle, |11\rangle\}$ . (b) Comparison of probabilities of the measurement outcomes for the pulse sequences shown in FIG. 9a and FIG. 9b for the input state  $|11\rangle$ .

From the transformations shown in Eq. 10, it can be verified that the unitary matrix  $U_B$  transforms the orthonormal product basis

$$\left\{ \frac{|00\rangle + |01\rangle}{\sqrt{2}}, \frac{|00\rangle - |01\rangle}{\sqrt{2}}, |10\rangle, |11\rangle \right\} \quad \text{into} \quad \text{maximally entangled two-qubit states. In the case of multi-qubits,}$$

there exist two inequivalent classes of genuinely entangled states: GHZ class and W class [15]. The GHZ state, representative of GHZ class, can be used for teleportation of a qubit [16] and superdense coding [17]. Similarly, perfect W states belonging W class can also be used for teleportation of a qubit and superdense coding [18]. Both the n-qubit GHZ state and n-qubit perfect W state can be generated by (n-1) applications of B-gate represented by the unitary matrix  $U_B$ . Circuits generating these states are shown in FIG. 11. The matrix representation of  $S^{\dagger}$ -gate [13] is

$$S^{\dagger} = \begin{bmatrix} 1 & 0 \\ 0 & -i \end{bmatrix} \tag{11}$$

The output of the circuit shown in Fig. 11a is the n-

qubit GHZ state up to a global phase,

$$|\text{GHZ}\rangle_n = \frac{e^{-i\pi/4}}{\sqrt{2}} \left[ \bigotimes_{j=1}^n |0\rangle_j + \bigotimes_{j=1}^n |1\rangle_j \right].$$
 (12)

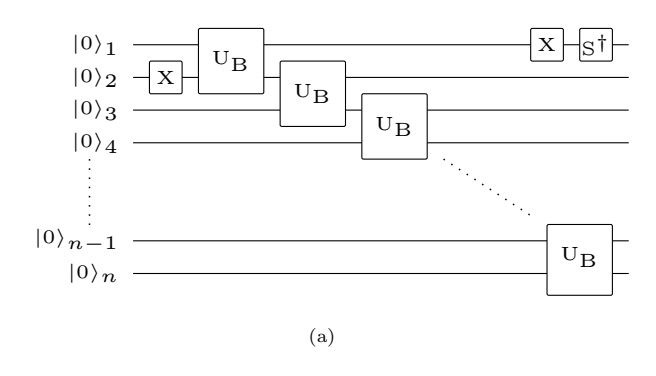
Similarly, the output of the circuit shown in Fig. 11b is the *n*-qubit perfect W state [19] up to a global phase,

$$|W_{\rm p}\rangle_n = \frac{e^{-i\pi/4}}{\sqrt{2}} \left[ |\Psi\rangle + |1\rangle_n \bigotimes_{j=1}^{n-1} |0\rangle_j \right],\tag{13}$$

where  $|\Psi\rangle$  is the normalized *n*-qubit state given as

$$|\Psi\rangle = \frac{e^{-i(n-2)\pi/4}}{2^{(n-2)/2}}|1\rangle_1 \bigotimes_{j=2}^n |0\rangle_j$$

$$+\sum_{k=2}^{n-1} \frac{ie^{-i(n-k)\pi/4}}{2^{(n-k)/2}} |1\rangle_k \bigotimes_{j=1, j \neq k}^n |0\rangle_j. \quad (14)$$



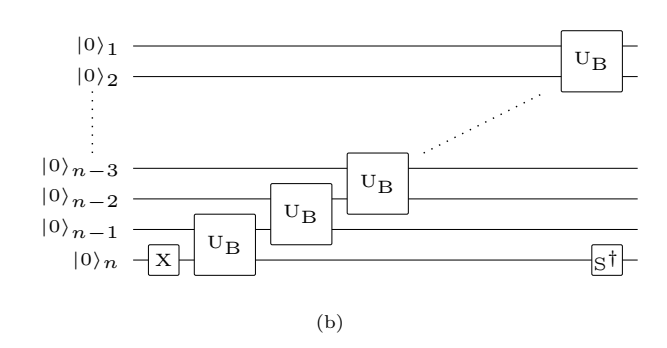


FIG. 11. Circuits generating (a) n-qubit GHZ state and (b) n-qubit Perfect W state.

To conclude, we have proposed a UTQQC that can be implemented using cross-resonance Hamiltonian. This circuit involves two applications of CNOT gate and two applications of a gate from  $[\text{CNOT}]^{\alpha}$  familiy with  $\alpha \in [0,0.5]$ . We have implemented a B-gate circuit using the pair  $\{\text{CNOT}, \sqrt{\text{CNOT}}\}$  and in this case, the implementation time is nearly 64.84% of the time required to implement the gate using two CNOT gates. When the  $\sqrt{\text{CNOT}}$  gate alone is used with single-qubit gates, it requires three applications of  $\sqrt{\text{CNOT}}$  gate to implement the B-gate [14]. Circuits consisting of (n-1) B-gates are constructed to generate n-qubit GHZ state and n-qubit perfect W state which are useful for teleportation

and superdense coding. Implementation of B-gate using the proposed UTQQC requires two CNOT and two  $\sqrt{\text{CNOT}}$  gates. Thus the implementation of many two-qubit gates using the proposed UTQQC will take more time in IBM quantum computers. However, an arbitrary two-qubit gate can be expressed by appending suitable single-qubit gates before and after the UTQQC. Thus using this proposed UTQQC an arbitrary two-qubit gate can be easily decomposed into implementable circuit. It only requires finding suitable single-qubit gates that have to be included at both ends of UTQQC.

**Acknowledgement:** We acknowledge the use of IBM Quantum services for this work. The views expressed are those of the authors, and do not reflect the official policy or position of IBM or the IBM Quantum team.

- M. A. Nielsen, C. M. Dawson, J. L. Dodd, A. Gilchrist, D. Mortimer, T. J. Osborne, M. J. Bremner, A. W. Harrow, and A. Hines, Phys. Rev. A, 67(5), p.052301 (2003)
- [2] Y. S. Zhang, M. Y. Ye, and G. C. Guo, Phys. Rev. A 71(6), 062331 (2005)
- [3] J. Zhang, J. Vala, S. Sastry, and K. B. Whaley, Phys. Rev. Lett. 93(2), 020502 (2004)
- [4] H. Fan, V. Roychowdhury, and T. Szkopek, Phys. Rev. A 72(5), 052323 (2005)
- [5] K. Selvan, and S. Balakrishnan, Eur. Phys. J. D 77, 144 (2023).
- [6] J. Zhang, J. Vala, S. Sastry, and K. B. Whaley, Phys. Rev. A 67(4), 042313 (2003)
- [7] J. P. Stenger, N. T. Bronn, D. J. Egger, and D. Pekker, Phys. Rev. Research, 3(3), 033171 (2021)
- [8] N. Earnest, C. Tornow, and D. J. Egger, Phys. Rev. Research, 3(4), 043088 (2021)
- [9] A. D. Córcoles, J. M. Gambetta, J. M. Chow, J. A. Smolin, M. Ware, J. Strand, B. L. T. Plourde, and M. Steffen, Phys. Rev. A, 87(3), 030301 (2013)
- [10] T. Alexander, N. Kanazawa, D. J. Egger, L. Capelluto, C. J. Wood, A. Javadi-Abhari, and D. C McKay, Quantum Sci. Technol. 5(4), 044006 (2020)

- [11] N. Sundaresan, I. Lauer, E. Pritchett, E. Magesan, P. Jurcevic, and J. M. Gambetta, PRX Quantum 1(2), 020318 (2020)
- [12] "IBM Quantum." https://quantum-computing.ibm.
- [13] "Qiskit: An open-source software for working with quantum computers at the level of circuits, pulses, and algorithms." https://qiskit.org/
- [14] T. Satoh, S. Oomura, M. Sugawara, and N. Yamamoto, IEEE Transactions on Quantum Engineering 3, pp. 1-10 (2022)
- [15] W. Dür, G. Vidal, and J. I. Cirac, Phys. Rev. A, 62(6), 062314 (2000)
- [16] A. Karlsson, and M. Bourennane, Phys. Rev. A, 58(6), 4394 (1998)
- [17] J. C. Hao, C. F. Li, and G. C. Guo, Phys. Rev. A, 63(5), 054301 (2001)
- [18] P. Agrawal, and A. Pati, Phys. Rev. A, 74(6), 062320 (2006)
- [19] M. Swain, M. K. Selvan, A. Rai, and P. K. Panigrahi, Quantum Inf Process., 22(8), 302 (2023)